

$BaTiO_3$/p-GaN/Au self-driven UV photodetector with bipolar photocurrent controlled by ferroelectric polarization

Wushuang Han(韩无双), Kewei Liu(刘可为), Jialin Yang(杨佳霖), Yongxue Zhu(朱勇学), Zhen Cheng(程祯), Xing Chen(陈星), Binghui Li(李炳辉), Lei Liu(刘雷), and Dezhen Shen(申德振)

Citation: Chin. Phys. B, 2024, 33 (**4**): 047701. DOI: 10.1088/1674-1056/ad2607
Journal homepage: http://cpb.iphy.ac.cn; http://iopscience.iop.org/cpb

What follows is a list of articles you may be interested in

SiC gate-controlled bipolar field effect composite transistor with polysilicon region for improving on-state current

Baoxing Duan(段宝兴), Kaishun Luo(罗开顺), and Yintang Yang(杨银堂)
Chin. Phys. B, 2023, 32 (**4**): 047702. DOI: 10.1088/1674-1056/ac80ab

Depolarization field in relaxor-based ferroelectric single crystals under one-cycle bipolar pulse drive

Chuan-Wen Chen(陈传文), Yang Xiang(项阳), Li-Guo Tang(汤立国), Lian Cui(崔莲), Bao-Qing Lin(林宝卿), Wei-Dong Du(杜伟东), Wen-Wu Cao(曹文武)
Chin. Phys. B, 2019, 28 (**12**): 127702. DOI: 10.1088/1674-1056/ab4e85

High uniformity and forming-free ZnO-based transparent RRAM with HfO_x inserting layer

Shi-Jian Wu(吴仕剑), Fang Wang(王芳), Zhi-Chao Zhang(张志超), Yi Li(李毅), Ye-Mei Han(韩叶梅), Zheng-Chun Yang(杨正春), Jin-Shi Zhao(赵金石), Kai-Liang Zhang(张楷亮)
Chin. Phys. B, 2018, 27 (**8**): 087701. DOI: 10.1088/1674-1056/27/8/087701

Microscopic degradation mechanism of polyimide film caused by surface discharge under bipolar continuous square impulse voltage

Luo Yang (罗杨), Wu Guang-Ning (吴广宁), Liu Ji-Wu (刘继午), Peng Jia (彭佳), Gao Guo-Qiang (高国强), Zhu Guang-Ya (朱光亚), Wang Peng (王鹏), Cao Kai-Jiang (曹开江)
Chin. Phys. B, 2014, 23 (**2**): 027703. DOI: 10.1088/1674-1056/23/2/027703

Bipolar resistive switching in $BiFe_{0.95}Zn_{0.05}O_3$ films

Yuan Xue-Yong (袁学勇), Luo Li-Rong (罗丽荣), Wu Di (吴迪), Xu Qing-Yu (徐庆宇)
Chin. Phys. B, 2013, 22 (**10**): 107702. DOI: 10.1088/1674-1056/22/10/107702

RAPID COMMUNICATION

$BaTiO_3$/p-GaN/Au self-driven UV photodetector with bipolar photocurrent controlled by ferroelectric polarization

Wushuang Han(韩无双)[1,2], Kewei Liu(刘可为)[1,2,†], Jialin Yang(杨佳霖)[1,2], Yongxue Zhu(朱勇学)[1,2], Zhen Cheng(程祯)[1,2], Xing Chen(陈星)[1,2], Binghui Li(李炳辉)[1,2], Lei Liu(刘雷)[1,2], and Dezhen Shen(申德振)[1,2]

[1] *State Key Laboratory of Luminescence and Applications, Changchun Institute of Optics, Fine Mechanics and Physics, Chinese Academy of Sciences, Changchun* 130033, *China*

[2] *Center of Materials Science and Optoelectronics Engineering, University of Chinese Academy of Sciences, Beijing* 100049, *China*

(Received 3 January 2024; revised manuscript received 29 January 2024; accepted manuscript online 5 February 2024)

Ferroelectric materials are promising candidates for ultraviolet photodetectors due to their ferroelectric effect. In this work, a $BaTiO_3$/p-GaN/Au hybrid heterojunction–Schottky self-driven ultraviolet photodetector was fabricated with excellent bipolar photoresponse property. At 0 V bias, the direction of the photocurrent can be switched by flipping the depolarization field of $BaTiO_3$, which allows the performance of photodetectors to be controlled by the ferroelectric effect. Meanwhile, a relatively large responsivity and a fast response speed can be also observed. In particular, when the depolarization field of $BaTiO_3$ is in the same direction of the built-in electric field of the Au/p-GaN Schottky junction (up polarized state), the photodetector exhibits a high responsivity of 18 mA/W at 360 nm, and a fast response speed of < 40 ms at 0 V. These findings pave a new way for the preparation of high-performance photodetectors with bipolar photocurrents.

Keywords: ferroelectric effect, bipolar, self-driven, photodetector

PACS: 77.55.fe, 77.80.–e, 85.60.–q, 61.80.Ba **DOI:** 10.1088/1674-1056/ad2607

1. Introduction

Self-driven ultraviolet (UV) photodetectors can convert UV light into electric signals without consuming any extra energy sources, which have broad potential applications in fields such as space exploration, flame detection, missile warning and optical communication.[1–7] In the past decades, wide-band-gap ferroelectric semiconductor materials, including $BiFeO_3$, $BaTiO_3$, $Pb(Zr,Ti)O_3$, $(Pb,La)(Zr,Ti)O_3$ (PLZT), etc, have been considered promising candidates for the preparation of self-driven UV photodetectors due to their unique ferroelectric polarization and photoelectric effects.[8–13] Most of the reported ferroelectric semiconductor UV photodetectors are based on a simple metal–ferroelectric material–metal structure, in which the photogenerated carriers are separated only/mainly through ferroelectric depolarization field to achieve self-driven operation.[10,14–17] Compared with traditional self-driven semiconductor photodetectors based on p–n or Schottky junctions, ferroelectric semiconductor devices can generate bipolar photocurrent by adjusting the direction of the ferroelectric depolarization field, which has a wide application prospect in optical communication, neuromorphic vision devices and logic circuits,[18–24] but they commonly suffer from the lower responsivity (10^{-7}–10^{-4} A/W).[25–29] To solve this problem, combining ferroelectric materials with other semiconductors to construct heterojunctions should be an effective approach and has been widely adopted recently.[18,30–32] For example, Chen *et al.* demonstrated a high-performance Au/ZnO/PLZT/FTO heterojunction-based self-driven UV photodetector with a responsivity of 3.96 mA/W at 360 nm by coupling the ferroelectric depolarization electric field and built-in electric field at the ZnO/PLZT interface.[33] Gao *et al.* achieved a high responsivity of 0.014 A/W in $SrTiO_3/TiO_2$ heterojunction photodetector under 375 nm light without external bias.[34] However, although the ferroelectric depolarization field can significantly improve the responsiveness of the self-driven device (up to tens of mA/W), it cannot change the direction of the photocurrent by controlling the direction of the ferroelectric polarization in the previously reported ferroelectric/semiconductor heterojunctions, which greatly hinders their applications in optical communication, neuromorphic vision devices, and logic circuits and computing. The main reason for the above problems should be that the strengths of the built-in electric field and the ferroelectric depolarization field at the ferroelectric/semiconductor interface in heterojunction devices are similar. When the directions of the ferroelectric field and the built-in electric field are the same, the light responsiveness can be significantly enhanced, but when the direction of the ferroelectric field is switched to the opposite direction, it is difficult to change the direction of the photocurrent. Therefore, it is challenging to achieve a self-driven bipolar UV photoresponse using simple ferroelectric/semiconductor heterojunctions.

Constructing a double-junction UV detector consisting of a ferroelectric/semiconductor heterojunction and a semi-

[†]Corresponding author. E-mail: liukw@ciomp.ac.cn

© 2024 Chinese Physical Society and IOP Publishing Ltd

conductor/metal Schottky junction is a feasible method to solve the above challenge. This double-junction device not only maintains the inherent advantages of ferroelectric/semiconductor heterojunction, but also cancels out the built-in electric field of the heterojunction to some extent by the additional semiconductor/metal Schottky junction. And thus the bipolar self-driven optical detection can be realized only by adjusting the direction of the ferroelectric depolarization field. GaN is one of the most popular wide bandgap semiconductors with excellent self-driven UV photodetection ability.[35–37] Meanwhile, $BaTiO_3$ is a typical n-type perovskite ferroelectric material with large spontaneous polarization generated by ferroelectricity. Therefore, under the guidance of the above idea, in this work, we fabricated a novel $BaTiO_3$/p-GaN/Au hybrid heterojunction–Schottky self-driven UV photodetector with excellent bipolar photoresponse properties. By modulating the direction of the depolarization field of $BaTiO_3$, photocurrents in different directions can be realized. At 0 V bias, when the depolarization field of $BaTiO_3$ is in the opposite direction of the built-in electric field of the $BaTiO_3$/p-GaN heterojunction, the responsivity of the device reaches 18 mA/W at 360 nm. Moreover, a fast response speed with rise/fall time of < 40 ms can be clearly observed with excellent repeatability and stability. The findings in this work provide a new idea for the preparation of high-performance bipolar self-driven photodetectors.

2. Experimental details

2.1. Preparation of the devices

The p-GaN film was grown on an undoped GaN (u-GaN)/sapphire substrate by molecular beam epitaxy (MBE). Subsequently, the $BaTiO_3$ film (3 mm diameter circle) was deposited on the p-GaN film covered with a Cu mask using magnetron sputtering. The deposited temperature, pressure and power were 500 °C, 1.2 Pa and 60 W, respectively. After that, a ring Au Schottky electrode was fabricated on the surface of the p-GaN film. Finally, the $BaTiO_3$/p-GaN/Au UV photodetector was demonstrated with indium (In) Ohmic contact on the $BaTiO_3$ film.

2.2. Characterizations of the materials and devices

The polarization–electric field (P–E) loop of $BaTiO_3$ was measured at a frequency of 2 Hz via a ferroelectric tester (Multiferroic 100, Radiant Technologies). The x-ray diffraction (XRD), electrical properties and the optical transmission spectra of the films were collected by a Bruker D8GADDS, a Lakeshore Hall effect measurement system and a scanning spectrophotometer (UV-3101PC), respectively. The morphology of the $BaTiO_3$/p-GaN heterojunction was investigated via a scanning electron microscope (SEM) (HITACHI S-4800). The current–voltage (I–V) curves and photoresponse properties of the photodetectors were tested using a semiconductor device analyzer (Agilent B1500A).

3. Results and discussion

Figures 1(a) and 1(b) show the surface and cross-sectional SEM images of $BaTiO_3$ deposited on the p-GaN film. The surface of the $BaTiO_3$ deposited on the p-GaN film is very flat and uniform, and the thicknesses of the $BaTiO_3$ and p-GaN films are approximately 600 nm and 100 nm, respectively. The AFM image of $BaTiO_3$ deposited on the p-GaN film is

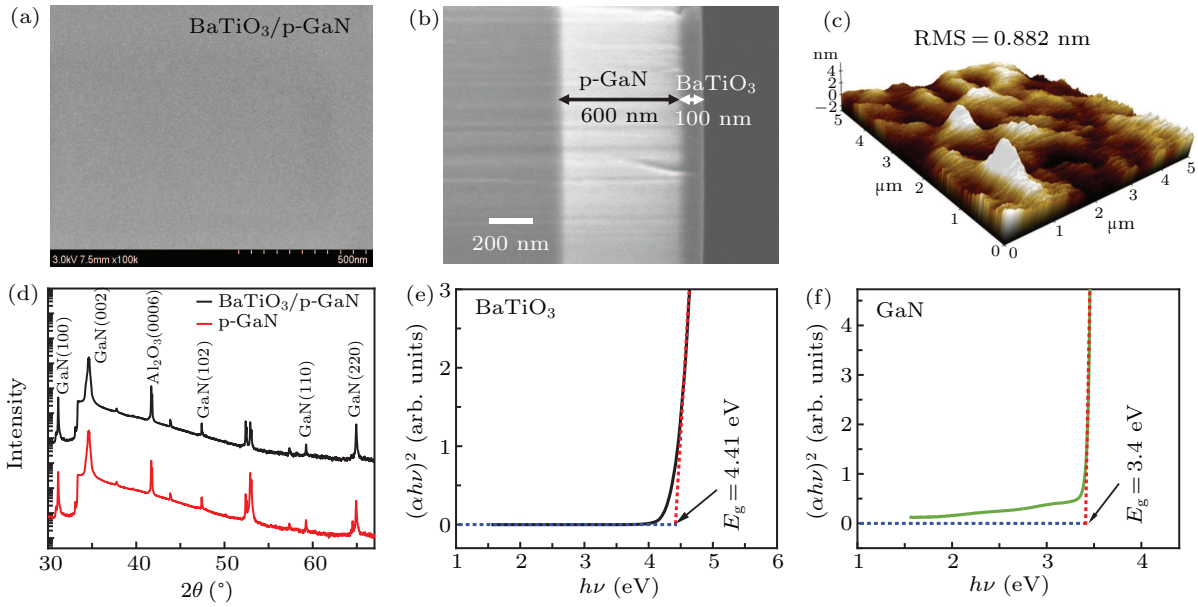


Fig. 1. (a) Top view and (b) cross-sectional SEM images, (c) AFM and (d) XRD patterns of the $BaTiO_3$ film deposited on p-GaN. The $(\alpha h\nu)^2$ as a function of $(h\nu)$ of the (e) $BaTiO_3$ deposited on sapphire and (f) p-GaN film deposited on u-GaN/sapphire.

shown in Fig. 1(c). The root mean square (RMS) surface roughness is found to be ∼ 0.882 nm. The XRD patterns suggest that $BaTiO_3$ film is amorphous as shown in Fig. 1(d). The binding energies of Ba^{2+}, Ti^{4+} and O^{2-} have been determined by the XPS spectra in our previous work, confirming the formation of $BaTiO_3$.[38] The carrier density and Hall mobility of the p-GaN film are 6.62×10^{18} cm^{-3} and 2.4 $cm^2/V{\cdot}s$, respectively. Figures 1(e) and 1(f) show the $(\alpha h\nu)^2$ as a function of $(h\nu)$ of the $BaTiO_3$ deposited on sapphire and p-GaN film deposited on u-GaN/sapphire, respectively. The bandgaps of the $BaTiO_3$ and GaN films are determined to be approximately 4.41 eV and 3.4 eV, respectively.

Figure 2(a) depicts the *P*–*E* hysteresis loop of the $BaTiO_3$ film at 2 Hz, which confirms its ferroelectric properties. The polarization of $BaTiO_3$ in the $BaTiO_3$/p-GaN/Au photodetector is achieved by applying ±40 V bias to the device for 200 s as shown in Fig. 2(b). In addition, the polarized states obtained after applying positive and negative voltages to the In electrode of the device are defined as the up polarized and down polarized states, respectively. In the up polarized state, the direction of the depolarization field (E_{dp}) in $BaTiO_3$ is the same as the built-in electric field of Schottky junction (E_s), while in the down polarized state, it is the same as the built-in electric field of the heterojunction (E_h). Figure 3(a) shows the photoresponse curves of the device in the un-polarized and polarized states under 365 nm light illumination at 0 V bias. Obviously, $BaTiO_3$/p-GaN/Au photodetector exhibits excellent self-driven performance, and reproducible and stable photocurrent to intermittent illumination. Moreover, the current of the photodetector in the up polarized state under 365 nm light illumination reaches 545 nA, which is significantly larger than that under un-polarized state. In contrast, in the down polarized state, the current of the device is −366 nA under 365 nm light illumination, and the current direction is opposite to that in the up polarized and un-polarized states. The response speeds of the $BaTiO_3$/p-GaN/Au photodetector in the polarized and un-polarized states are estimated at 0 V as presented in Fig. 3(b). Obviously, the 10%–90% rise time (t_r) and the 90%–10% fall time (t_f) are determined to be less than 40 ms (instrumental detection limit) in all three states, indicating that the device has a fast response speed. Figure 3(c) presents the pulse-switching characteristics of the $BaTiO_3$/p-GaN/Au device. It is obvious that the device in the un-polarized state shows a weak response to the UV light at room temperature. When a positive or negative voltage pulse (±40 V, 200 s) is applied to the device, the device would change from an un-polarized state to a polarized state, and the direction and intensity of the photocurrent can be effectively controlled. Moreover, after heating at 130 °C for 300 s, the photocurrent decreases sharply and the device returns to the un-polarized state. The photocurrents of the device in up and down polarized states show insignificant deterioration after 50 voltage pulse cycles (±40 V, 200 s) in Fig. 3(d). Figure 3(e) shows the spectral response of the photodetector at 0 V bias in the up polarized state. The highest responsivity (*R*) of the device is observed at approximately 360 nm, reaching 18 mA/W. The UV-to-visible rejection ratio (R_{360}/R_{400}) is 1.5×10^2, indicating the excellent spectral selectivity.

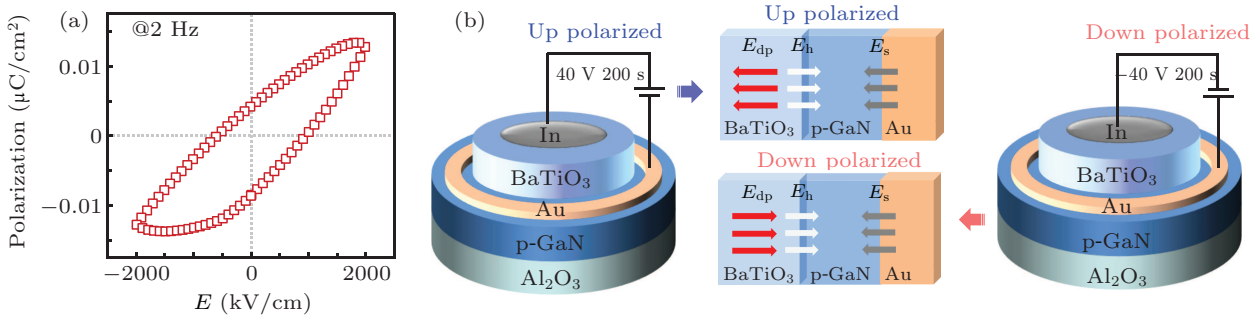


Fig. 2. (a) The *P*–*E* loop of the $BaTiO_3$ film measured at 2 Hz. (b) Schematic illustrations of photodetector in the up polarized and down polarized states.

Notably, the magnitude and direction of photocurrent of the photodetector strongly depend on the polarization direction. To better understand the mechanism for the above phenomenon, the energy band diagram and schematic diagram of the $BaTiO_3$/p-GaN/Au hybrid structure in different polarized states under UV light illumination at 0 V are depicted in Figs. 4 and 5. The electron affinity of GaN and $BaTiO_3$ is 2.1 eV and 1.3 eV, [38,39] respectively. The bandgap is 3.4 eV and 4.41 eV for p-GaN and $BaTiO_3$, respectively. When the device is in the un-polarized state (see Fig. 4(b) and the upper part of Fig. 5), the built-in electric field directions of the heterojunction (E_h) and the Schottky junction (E_s) are opposite, and the contribution of E_s to photocurrent is greater than that of E_h, so the device shows a weak photocurrent in the same direction as E_s under 365 nm light irradiation. Once the device is in the up polarized state as shown in Fig. 4(c) and the left

side of Fig. 5, the depolarization field (E_{dp}) in $BaTiO_3$ is in the opposite direction of E_h, which weakens the separation of the photogenerated carriers in the depletion region of the heterojunction, thus increasing the photocurrent. On the contrary, when the device is in the down polarized state (see Fig. 4(d) and the right side of Fig. 5), the direction of E_{dp} is the same as E_h, which improves the separation and transport of the photogenerated carriers. Meanwhile, the contribution of E_{dp} and E_h to the photocurrent is greater than that of E_s, and thus the photocurrent direction of the device can be reversed.

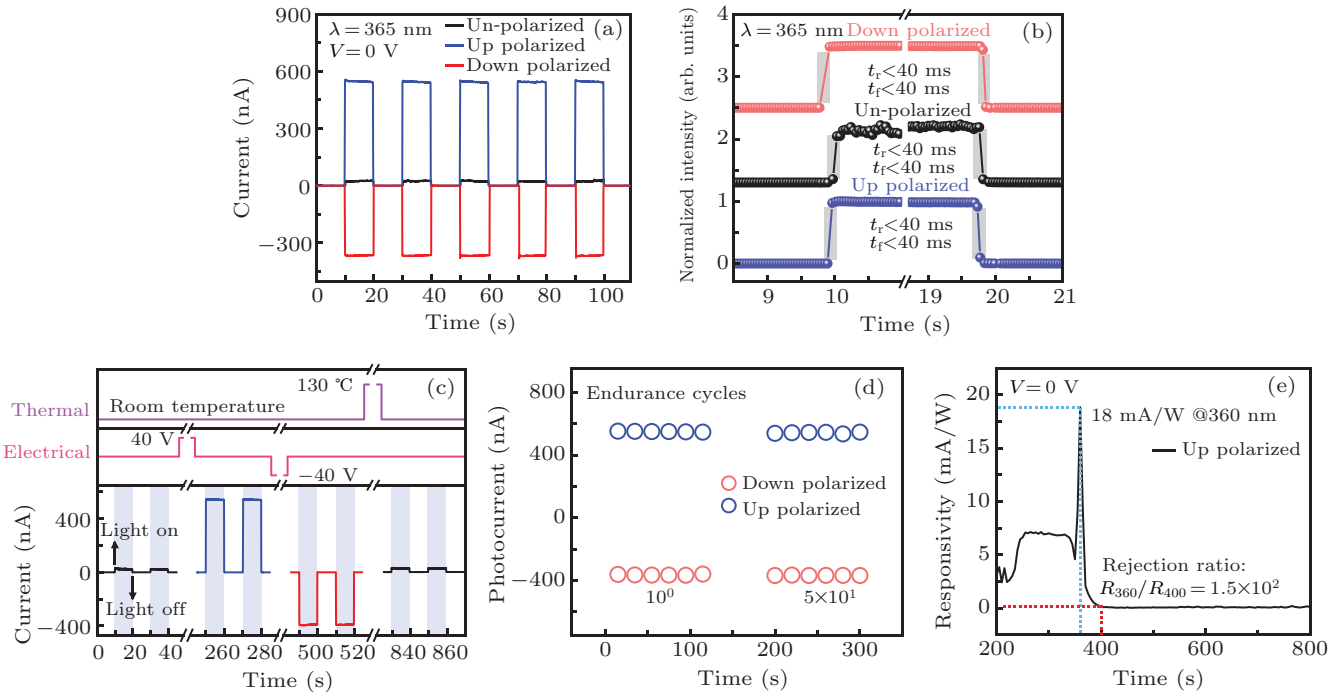


Fig. 3. (a) Photoresponse characteristics of $BaTiO_3$/p-GaN/Au photodetector in un-polarized and polarized states under 365 nm light illumination at 0 V bias. (b) A single cycle photoresponse, (c) pulse-switching characteristics, (d) photocurrent after different endurance cycles and (e) spectral response of the photodetector.

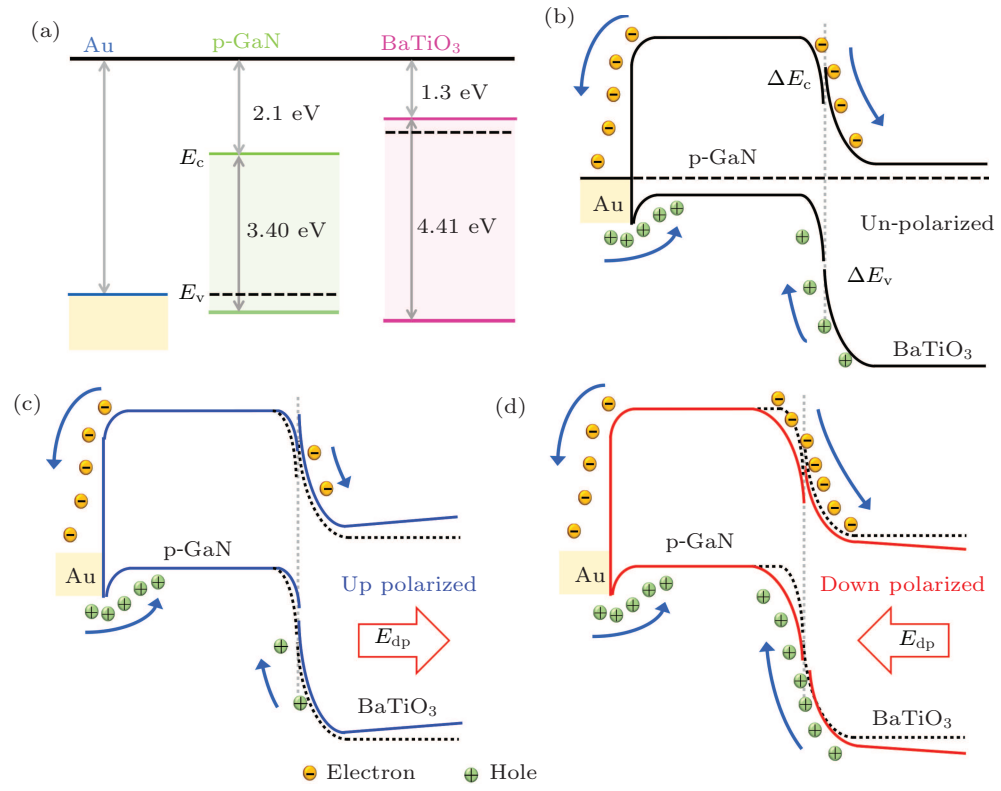


Fig. 4. The band-structure and energy band diagram of the photodetector in un-polarized, up and down polarized states.

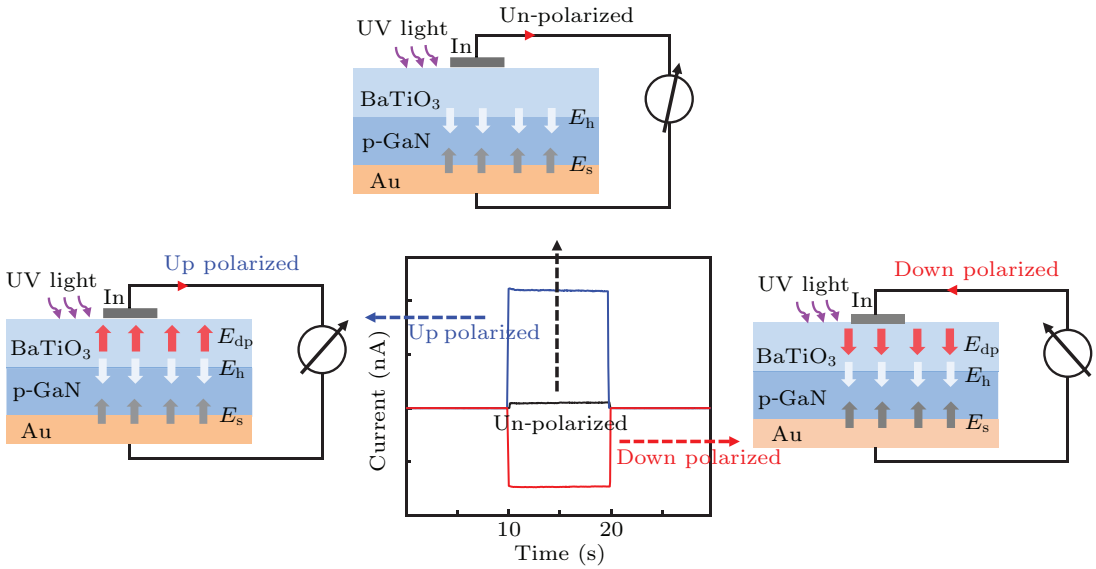


Fig. 5. Schematic illustrations of the photodetector at un-polarized and polarized states.

Table 1. The representative works of the ferroelectric/semiconductor heterojunction and bipolar self-driven photodetectors.

Device structure	Bipolar device	Bias (V)	Wavelength (nm)	t_r/t_f (s)	Responsivity (A/W)	Ref.
Au/ZnO/PLZT/FTO	no	0	360	0.4/1.6	3.96×10^{-3}	[33]
ZnO/$BaTiO_3$	no	0	368	0.04/0.05	1.41×10^{-3}	[30]
ITO/NiO/PLZT/FTO	no	0	350	0.34/0.36	1.8×10^{-4}	[18]
Au/PZT/$CuBi_2O_4$/ITO	no	0	425	–/–	2.4×10^{-4}	[19]
ZnO/$BiFeO_3$	no	0	420	0.127/0.449	1.32×10^{-3}	[40]
$BaTiO_3$/p-Si	no	0	365	6×10^5/1.4×10^{-4}	2.7×10^{-2}	[38]
Au/$BaTiO_3$/Au	yes	0	320	2×10^{-10}	1×10^{-5}	[25]
Au/$BiFeO_3$/Au	yes	0	365	$1.18/23.6\times10^{-8}$	1.5×10^{-4}	[27]
Pt/DJ-OIHP(AMP)(MA)Pb_2I_7/Pt	yes	0	532	0.4	1.61×10^{-4}	[41]
$BaTiO_3$/p-GaN/Au	yes	0	365	< 0.4	1.8×10^{-2}	this work

Table 1 shows the comparison of the performance parameters of our $BaTiO_3$/p-GaN/Au hybrid structure device with those of the reported self-driven photodetectors based on ferroelectric/semiconductor heterojunctions and pure ferroelectric materials. This $BaTiO_3$/p-GaN/Au device can be operated at 0 V with excellent bipolar photoresponse properties. More importantly, the responsivity of our device is significantly higher than that of most previously reported self-driven photodetectors, while its response time is comparable. This provides a feasible route for the application of photodetectors with double-junction in the fields of optical communications, neuromorphic vision devices, and logic circuits and computing.

4. Conclusion

In summary, a self-driven $BaTiO_3$/p-GaN/Au bipolar UV photodetector was prepared in this work. The photocurrent direction can be switched by adjusting the direction of the depolarization field of $BaTiO_3$. The built-in electric fields with similar intensity and opposite direction of $BaTiO_3$/p-GaN heterojunction and Au/p-GaN Schottky junction in the device, and the controlled ferroelectric depolarization field in the $BaTiO_3$ can be used to explain the above phenomenon. When the depolarization field of $BaTiO_3$ is in the same direction of the built-in electric field of the Au/p-GaN Schottky junction (up polarized state) and $BaTiO_3$/p-GaN heterojunction (down polarized state), the currents of the photodetector under 365 nm light illumination are around 545 nA and −366 nA, respectively. The device in the up polarized state exhibited a high peak responsivity of 18 mA/W at 360 nm and a fast response speed with t_r/t_f of < 40 ms at 0 V bias. This work indicates that hybrid-structure devices based on ferroelectric materials and semiconductors are promising candidates for the application in optical communication, neuromorphic vision devices, and logic circuits.

Acknowledgements

Project supported by the National Natural Science Foundation of China (Grant Nos. 62074148, 61875194, 11727902, 12204474, 12304111, and 12304112), the Youth Innovation Promotion Association, Chinese Academy of Sciences (Grant No. 2020225), Jilin Province Science Fund (Grant Nos. 20220101053JC and 20210101145JC), and Jilin Province Young and Middle-Aged Science and

Technology Innovation Leaders and Team Project (Grant No. 20220508153RC).

References

[1] Hou H Y, Tian S, Chen J D, Ling H H, Ren H, Zhang Y F, Ge H R, Chen W S, Li Y Q, Mao H Y, Ishii H and Tang J X 2023 *Advanced Optical Materials*

[2] Kumar M, Park J Y and Seo H 2021 *ACS Applied Materials & Interfaces* **13** 12241

[3] Gao L, Chen C, Zeng K, Ge C, Yang D, Song H S and Tang J 2016 *Light-Science & Applications* **5** e16126

[4] Li C L, Wang H L, Wang F, Li T F, Xu M J, Wang H, Wang Z, Zhan X W, Hu W D and Shen L 2020 *Light-Science & Applications* **9** 31

[5] Yang J, Liu K, Chen X and Shen D 2022 *Progress in Quantum Electronics* **83** 100397

[6] Li K, Xu L, Lu Q D and Hu P 2023 *Chin. Phys. B* **32** 118503

[7] Yang L L, Peng Y S, Liu Z, Zhang M L, Guo Y F, Yang Y and Tang W H 2023 *Chin. Phys. B* **32** 047301

[8] Qi J, Ma N, Ma X C, Adelung R and Yang Y 2018 *ACS Applied Materials & Interfaces* **10** 13712

[9] Li Z, Zhao Y, Li W L, Peng Y Z, Zhao W Y, Wang Z, Shi L and Fei W D 2022 *Journal of Materials Chemistry A* **10** 8772

[10] Ma N and Yang Y 2017 *Nano Energy* **40** 352

[11] Song K, Ma N and Yang Y 2017 *Advanced Materials Technologies* **2** 1700221

[12] Chen J, Priya A S, You D, Pei W J, Zhang Q F, Lu Y M, Li M K, Guo J M and He Y B 2020 *Sensors and Actuators A-Physical* **315** 112267

[13] Gan B K, Yao K, Lai S C, Goh P C and Chen Y F 2011 *IEEE Electron Device Lett.* **32** 665

[14] Zhao R, Ma N, Song K and Yang Y 2020 *Adv. Funct. Mater.* **30** 1906232

[15] Qi J, Ma N and Yang Y 2018 *Advanced Materials Interfaces* **5** 142901

[16] Song K, Ma N, Mishra Y K, Adelung R and Yang Y 2019 *Advanced Electronic Materials* **5** 1800413

[17] Ma N, Zhang K W and Yang Y 2017 *Adv. Mater.* **29** 10

[18] Chen J, You D, Zhang Y, Zhang T, Yao C, Zhang Q F, Li M K, Lu Y M and He Y B 2020 *ACS Applied Materials & Interfaces* **12** 53957

[19] Ashtar M, Marwat M A, Li Z T, Yang Y and Cao D W 2023 *Journal of Luminescence* **260** 119855

[20] Wu G J, Zhang X M, Feng G D, Wang J L, Zhou K J, Zeng J H, Dong D N, Zhu F D, Yang C K, Zhao X M, Gong D N, Zhang M R, Tian B B, Duan C A, Liu Q, Chu J H and Liu M 2023 *Nat. Mater.*

[21] Wu G J, Tian B B, Liu L, Lv W, Wu S, Wang X D, Chen Y, Li J Y, Wang Z, Wu S Q, Shen H, Lin T, Zhou P, Liu Q, Duan C G, Zhang S T, Meng X J, Wu S W, Hu W D, Wang X R, Chu J H and Wang J L 2020 *Nat. Electron.* **3** 43

[22] Wu G J, Wang X D, Chen Y, Wu S Q, Wu B M, Jiang Y Y, Shen H, Lin T, Liu Q, Wang X R, Zhou P, Zhang S T, Hu W D, Meng X J, Chu J H and Wang J L 2020 *Adv. Mater.* **32** 1907937

[23] Chen S S, Zhang X H, Wang G C, Chen S, Ma H Q, Sun T Y, Man B Y and Yang C 2023 *Chin. Phys. B* **32** 127301

[24] Ou Y J, Sun J, Li Y M and Jiang A Q 2023 *Chin. Phys. Lett.* **40** 038501

[25] Li J K, Ge C, Jin K J, Du J Y, Yang J T, Lu H B and Yang G Z 2017 *Appl. Phys. Lett.* **110** 142901

[26] Li C X, Chen C, Zhao L and Ma N 2023 *ACS Applied Materials & Interfaces* **15** 23402

[27] Xing J, Guo E J, Dong J J, Hao H Y, Zheng Z Y and Zhao C C 2015 *Appl. Phys. Lett.* **106** 033504

[28] Kim W, Kim H, Yoo T J, Lee J Y, Jo J Y, Lee B H, Sasikala A A, Jung G Y and Pak Y 2022 *Nat. Commun.* **13** 720

[29] Li M, Sun H, Ruan Y, Cao C, Zhou P, Qi Y and Zhang T 2023 *Applied Surface Science* **618** 156665

[30] Yu P, Wang W, Zheng T, Wan X and Jiang Y 2023 *ACS Applied Materials & Interfaces* **15** 46031

[31] Wang S, Nan F, Zhou Y, Zheng F G, Weng Y Y, You L and Fang L 2020 *J. Appl. Phys.* **128** 154101

[32] Zhang Y, Chen J, Zhang Q, Lu Y, Huang H and He Y 2022 *J. Am. Ceram. Soc.* **105** 392

[33] Chen J, Wang Z H, He H F, Mao J X, Zhang Y, Zhang Q F, Li M K, Lu Y M and He Y B 2021 *Advanced Electronic Materials* **7** 2100717

[34] Gao S Y, Xu J P, Shi S B, Chen J, Xu J H, Kong L N, Zhang X S and Li L 2023 *J. Mater. Chem. C* **11** 9201

[35] Hu T G, Zhao L X, Wang Y J, Lin H L, Xie S H, Hu Y, Liu C, Zhu W K, Wei Z M, Liu J and Wang K Y 2023 *ACS Nano* **17** 8411

[36] Liu C, Li X D, Hu T G, Zhu W K, Yan F G, Wu T S, Wang K Y and Zhao L X 2021 *Nanoscale* **13** 17512

[37] Li J, Xi X, Lin S, Ma Z H, Li X D and Zhao L X 2020 *ACS Applied Materials & Interfaces* **12** 11965

[38] Han W S, Liu K W, Yang J L, Chen X, Ai Q, Zhu Y X, Cheng Z, Li B H, Liu L and Shen D Z 2023 *Applied Surface Science* **615** 156371

[39] Wu C I and Kahn A 2000 *Applied Surface Science* **162** 250

[40] Zhou X, Xu J P, Shi S B, Chen J, Xu J H, Kong L N, Zhang X S and Li L 2023 *Applied Surface Science* **623** 157032

[41] Park I H, Kwon K C, Zhu Z Y, Wu X, Li R L, Xu Q H and Loh K P 2020 *J. Am. Chem. Soc.* **142** 18592